RSC Advances

PAPER

View Article Online
View Journal | View Issue

Cite this: *RSC Adv.*, 2023, **13**, 26851

Comparative study of distinct halide composites for highly efficient perovskite solar cells using a SCAPS-1D simulator

Sagar Bhattarai, *[ab] Rahul Pandey, *[c] Jaya Madan,*[c] Soney Tayeng,[b] P. K. Kalita,[d] Mohd Zahid Ansari, *[e] Lamia Ben Farhat,[f] Mongi Amami[f] and M. Khalid Hossain *[g]

This research investigates the influence of halide-based methylammonium-based perovskites as the active absorber layer (PAL) in perovskite solar cells (PSCs). Using SCAPS-1D simulation software, the study optimizes PSC performance by analyzing PAL thickness, temperature, and defect density impact on output parameters. PAL thickness analysis reveals that increasing thickness enhances J_{SC} for $MAPbI_3$ and $MAPbI_2Br$, while that of $MAPbBr_3$ remains steady. V_{OC} remains constant, and FF and PCE vary with thickness. $MAPbI_2Br$ exhibits the highest efficiency of 22.05% at 1.2 μm thickness. Temperature impact analysis shows J_{SC}, V_{OC}, FF, and PCE decrease with rising temperature. $MAPbI_2Br$-based PSC achieves the highest efficiency of 22.05% at 300 K. Contour plots demonstrate that optimal PAL thickness for the $MAPbI_2Br$-based PSC is 1.2 μm with a defect density of 1×10^{13} cm^{-3}, resulting in a PCE of approximately 22.05%. Impedance analysis shows the $MAPbBr_3$-based PSC has the highest impedance, followed by Cl_2Br-based and I-based perovskite materials. A comparison of QE and *J*–*V* characteristics indicates $MAPbI_2Br$ offers the best combination of V_{OC} and J_{SC}, resulting in superior efficiency. Overall, this study enhances PSC performance with $MAPbI_2Br$-based devices, achieving an improved power conversion efficiency of 22.05%. These findings contribute to developing more efficient perovskite solar cells using distinct halide-based perovskite materials.

Received 21st June 2023
Accepted 17th August 2023

DOI: 10.1039/d3ra04134d

rsc.li/rsc-advances

1. Introduction

After decades of research to improve the power consumption efficiency (PCE) of renewable solar cells, which can effectively substitute the depleting fossil fuels, perovskite solar cells (PSCs) have seen a significant increase in efficiency in the last decade, as evidently studied by many researchers.[1–5] Their remarkable properties, which include a very high absorption coefficient, a tunable band gap, an extended diffusion length of the carriers, greater mobility of charge, a lower trap state density, a smaller binding energy of the excitons, and a low processing cost, have enabled them to achieve this feat.[6–11] The chemical formula for perovskite is PQX_3, where P stands for an organic/inorganic cation (Cs or MA or FA), Q stands for heavy metals (Sn, Ge, Pb), and X shows the halide anions (Br, Cl, and I).[12–15] More specifically, the organic–inorganic perovskites have blazed a trail toward a highly efficient light-harvesting material and the PSC efficiency has now increased from 3% to 25.6%.[16–20] Because of the tunable frequency, the PCSs can absorb different light frequencies effectively in different layers, improving PCE.[21–26]

Many previous studies have been conducted on perovskite materials consist of Pb, which are the most efficient and reliable.[27] These PSCs have their own set of advantages and disadvantages, such as high efficiency and stability but poor performance, high stability but not eco-friendly, and so on.[28–34] These issues can be addressed through improved engineered devices, encapsulation, and the use of 2D perovskites. Milot *et al.* verified that $FASnI_3$ had higher carrier mobility, lower auger recombination rate constants, and a more substantial radiative rate of recombination constant that is comparable to GaAs.[35] While Lee *et al.* combined $FASnI_3$ with the SnF_2–pyrazine complex to slow the crystallization and also attain a PCE up to 4.8%.[36] Ban *et al.* fabricated an 8.03% efficient $CsSnI_3$ absorber layer-based PSCs with V_{OC} of 520 mV and J_{SC} of 23.4%.[37] The work by Abdelaziz *et al.*, where they used SCAPS software to investigate how the thickness, the defect density, and the doping affect the device output of $[HC(NH_2)_2$-SnI_3-

[a]*Technology Innovation and Development Foundation, Indian Institute of Technology Guwahati, Guwahati 781039, Assam, India. E-mail: sagarbhattarai012@gmail.com*
[b]*Department of Physics, Arunachal University of Studies, Namsai, Arunachal Pradesh, 792103, India*
[c]*VLSI Centre of Excellence, Chitkara University Institute of Engineering and Technology, Chitkara University, Punjab 140401, India. E-mail: rahul.pandey@chitkara.edu.in; Jaya.madan@chitkara.edu.in*
[d]*Department of Physics, Rajiv Gandhi University, Arunachal Pradesh 791112, India*
[e]*School of Materials Science and Engineering, Yeungnam University, Gyeongbuk 38541, Republic of Korea*
[f]*Department of Chemistry, College of Sciences, King Khalid University, P.O. Box 9004, Abha, Saudi Arabia*
[g]*Institute of Electronics, Atomic Energy Research Establishment, Bangladesh Atomic Energy Commission, Dhaka 1349, Bangladesh. E-mail: khalid.baec@gmail.com; khalid@kyudai.jp*

FASnI$_3$] based PSCs that achieves a PCE up to 14.03%, V_{OC} of 0.92 V, and J_{SC} of 22.65 mA cm^{-2} and a FF of 67.74%.[38]

Certain studies have been reported to discover the characteristics of the PSCs. Such research is required to better understand perovskites and capitalize on their advantages. The results of these studies will provide valuable insights that will allow us to make informed decisions about how to use perovskite solar cells at best.[39–41] The methylammonium-based PSC offered the most predominant efficiency, starting from 16% to 20% by Cao *et al.* and Bhattarai *et al.*[42,43] The efficiency reached up to 22.16% in the recent numerical simulation study.[42] It is crucial to investigate perovskites with exceptional optical and

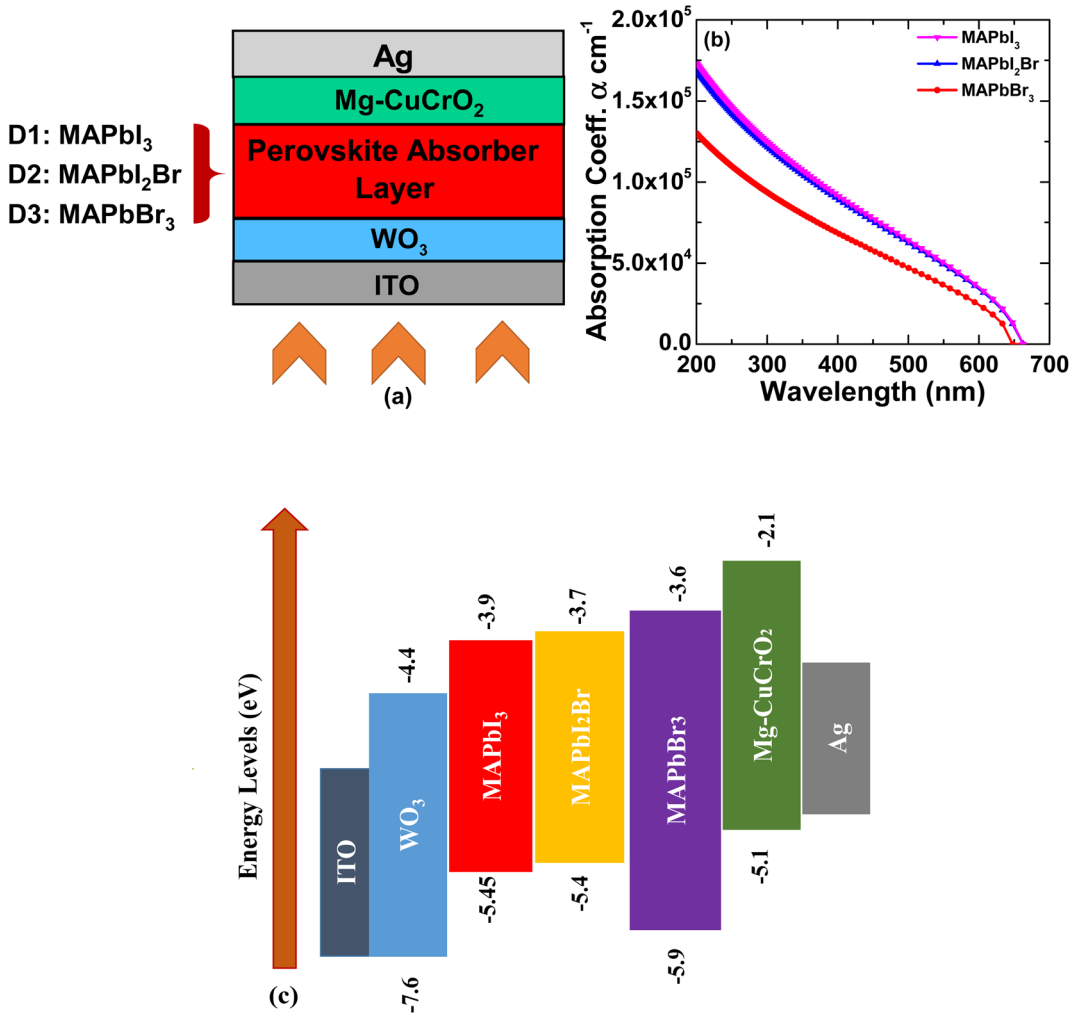

Fig. 1 (a) The proposed architecture of MA-based PSC, (b) absorption coefficient of perovskite materials under the illuminance of AM1.5G, and band energy diagram of PSCs.

Table 1 The inputs in the simulated PSC device[27,44–48]

Parameters	Terms	ETL (WO_3)	PAL$_1$ ($MAPbI_3$)	PAL$_2$ ($MAPbBr_3$)	PAL$_3$ ($MAPbI_2Br$)	HTL ($Mg–CuCrO_2$)
d (μm)	Thicknesses	0.1–0.15	0.2–1.2	0.2–1.2	0.2–1.2	0.1–0.15
E_g (eV)	Bandgap	3.2	1.55	2.3	1.7	3.0
ε_r	Relative permittivity	9	6.5	6.5	15	9.5
χ (eV)	Electron affinity	4.4	3.9	3.6	3.7	2.1
N_c (cm^{-3})	Eff. DoS at CB.	1×10^{20}	2.2×10^{18}	2.2×10^{18}	3×10^{17}	1×10^{19}
N_v (cm^{-3})	Eff. DoS at VB.	2×10^{21}	1.8×10^{18}	1.8×10^{19}	4×10^{18}	1×10^{19}
μ_n (cm^2 V^{-1} s^{-1})	Mobility of e	100	2	20	15	0.1
μ_p (cm^2 V^{-1} s^{-1})	Mobility of h	25	2	20	15	2.53
D_a (cm^{-3})	Dop. den. of the acceptor	0	5.21×10^9	0	0	6.4×10^{15}
D_d (cm^{-3})	Dop. den. of donor	1×10^{21}	5.21×10^9	0	1×10^{16}	0
N_t (cm^{-3})	Def. density	1×10^{14}	1×10^{13}	1×10^{13}	1×10^{13}	1×10^{14}

Table 2 Parameter of interface defects used in simulations

Parameters	Mg–$CuCrO_2$/PALs	PALs/WO_3
Defect types	Neutral	Neutral
e cap. cross-section (cm^2)	1×10^{-19}	1×10^{-19}
h cap. cross-section (cm^2)	1×10^{-19}	1×10^{-19}
Energy distributions	Single	Single
Ref. for def. energy levels	Above the highest EV	Above the highest EV
Energy with respect to ref. (eV)	0.6	0.6
Total density (integrated over all energies) (cm^{-2})	1×10^9	1×10^9

electrical properties in order to achieve a balance between stability and performance. So, there is still a huge scope to study with the help of simulation to fully understand these materials' distinct properties and associated performance parameters. Further, among the various types of perovskite materials, $MAPbI_{3-x}Br_x$, a hybrid organic–inorganic lead halide perovskite, has garnered significant attention as an absorber layer in PSCs. This compound offers a versatile platform for developing efficient and stable solar cells, holding great potential for revolutionizing the renewable energy landscape. $MAPbI_{3-x}Br_x$ is a solid solution of methylammonium lead iodide ($MAPbI_3$) and methylammonium lead bromide ($MAPbBr_3$). The incorporation of bromine (Br) atoms into the $MAPbI_3$ lattice allows for the controlled modification of its composition and bandgap. By fine-tuning the ratio of iodine (I) to bromine (Br) atoms, the bandgap of $MAPbI_{3-x}Br_x$ can be engineered to match specific solar spectra, optimizing light absorption and enhancing device efficiency. One of the key advantages of utilizing $MAPbI_{3-x}Br_x$ in PSCs is its high absorption coefficient, enabling efficient utilization of a broad range of solar wavelengths. This exceptional light-harvesting capability results in higher photocurrents and improved overall energy conversion efficiency. Furthermore, the energy levels of $MAPbI_{3-x}Br_x$ align favourably with the other functional layers within the PSC device, facilitating efficient charge transport and minimizing recombination losses.

Therefore, extensive PV study related to $MAPbI_{3-x}Br_x$ at varying halide compositions is much needed to comprehend the influence of different halide compositions on the outputs of the PSC. Therefore, in this work, the primary intent is to investigate and compare the properties of various Perovskite materials concerning their different halide materials in relation to their performance parameters. A comparative study of various perovskites, such as $MAPbI_3$, $MAPbI_2Br$, and $MAPbBr_3$, is carried out to help us to apprehend the distinct performances and the influence on the output parameters and to additional work for highly efficient and more suitable stable perovskite.

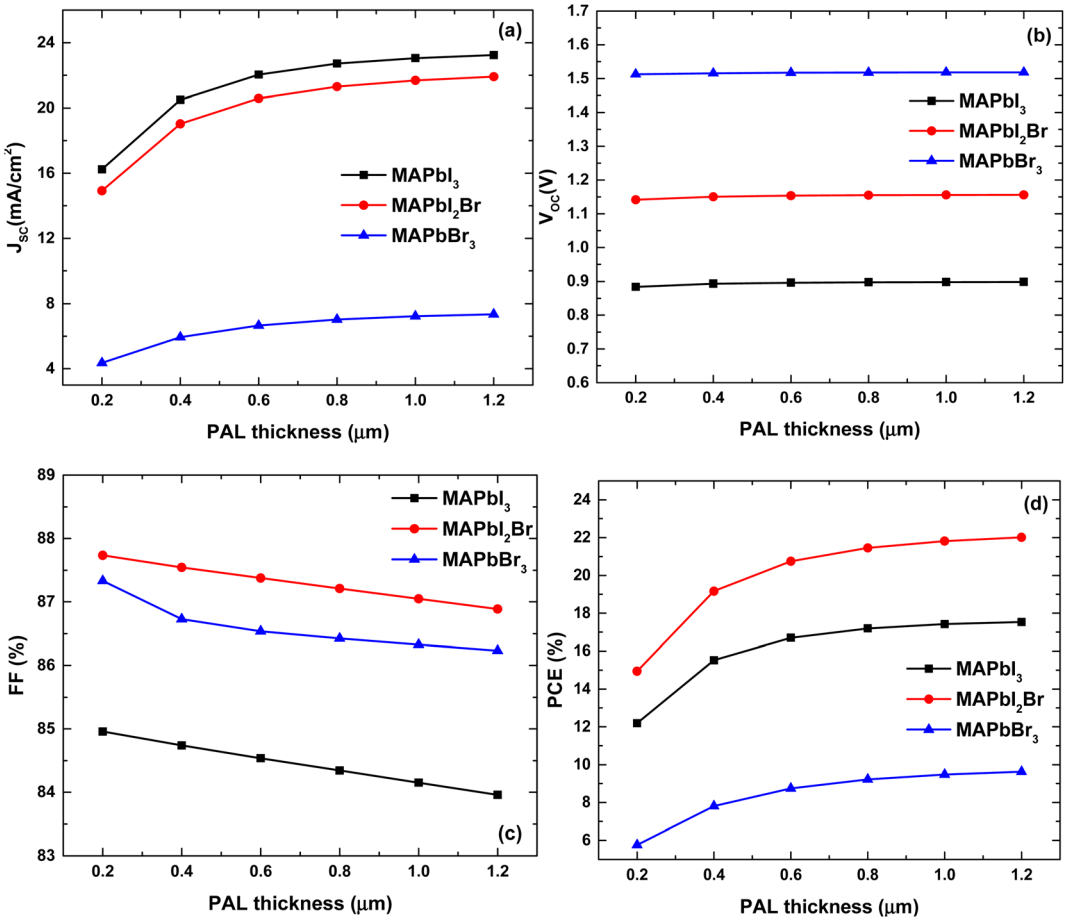

Fig. 2 The impact of the perovskite thicknesses on the outputs of the PSC devices.

2. Device configurations

In Fig. 1a, the heterojunction PSCs with the ITO/ETL/perovskite/HTL/Ag device configuration are used to simulate PSC devices. More specifically, a 0.1 μm top anode of ITO is placed after a 0.1 μm WO_3 layer in the simulated PSC devices, which serves as the ETL and effectively channels the produced electrons from the absorber layers in the PSC device. The HTL of Mg–$CuCrO_2$ is placed having a thickness of 0.1 μm. The material is used due to its appropriate band alignment with the perovskite absorber. During device fabrication, Mg–$CuCrO_2$-based HTL can be fabricated using different deposition techniques such as spin-coating, doctor-blading, spray-coating, or inkjet printing. The perovskite absorber layer (PAL) for the devices is 0.4 μm thick and is sandwiched between an HTL and an ETL. The holes generated in the PSC are successfully collected and transferred to the cathode by the hooping mechanism. The cathode is made of 0.1 μm thicker Ag material, which is cheaper than other cathode materials such as Gold (Au). Table 1 and 2 list all of the input parameters used by the PSC device and interface defectivity details, respectively.

In Fig. 1b, the perovskites, namely $MAPbI_3$, $MAPbI_2Br$, and $MAPbBr_3$, are shown with their respective coefficients over the wavelengths. The absorption coefficients are obtained from the simulating software of SCAPS-1D.[49–63] On the other hand, the band energy diagram for all the possible constituent layers in the three designs of the perovskites is also depicted in Fig. 1c, respectively.

3. Results and discussion

The discussion in this part is only focused on the findings and analysis of the current study. The results and discussion segment comprise five smaller portions, numbered 3.1 to 3.5. First, if appropriate, a bandgap analysis is performed, followed by impacts on absorber thickness, temperature, and overall defect density. In this part, the contour analysis for the MA-based solar cell has also been studied simultaneously.

The work is simulated at 300 K temperature to check the band alignment of the PSC device and obtain the desired results. The following is a detailed investigation of the current work.

3.1 The influence of PAL-thickness in outputs of the PSC

Thickness tuning of the PSC constituent layer is one of the most promising and successful methods for increasing the effectiveness of the PSC device. The PSC was thickened from 0.2–1.2

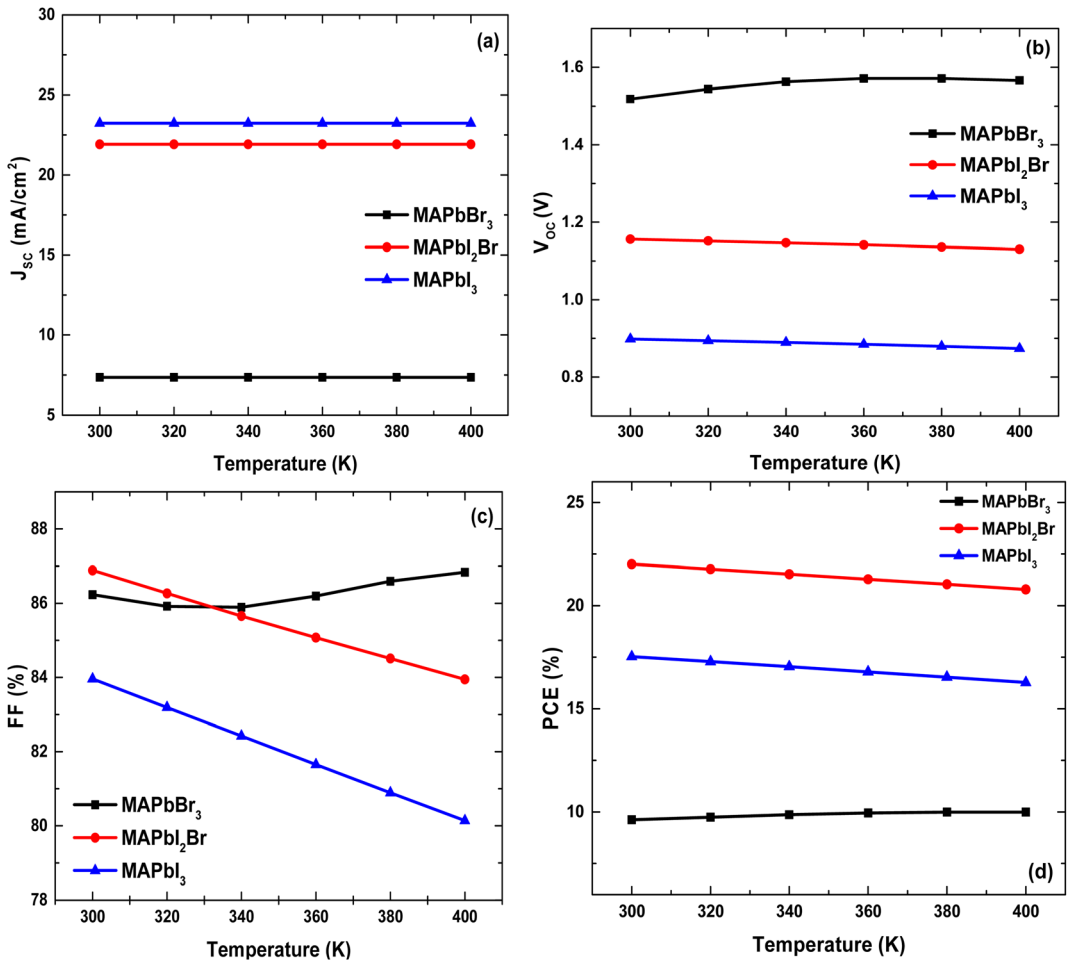

Fig. 3 The influence of temperature on the PV parameters of the PSC at the optimized thickness conditions.

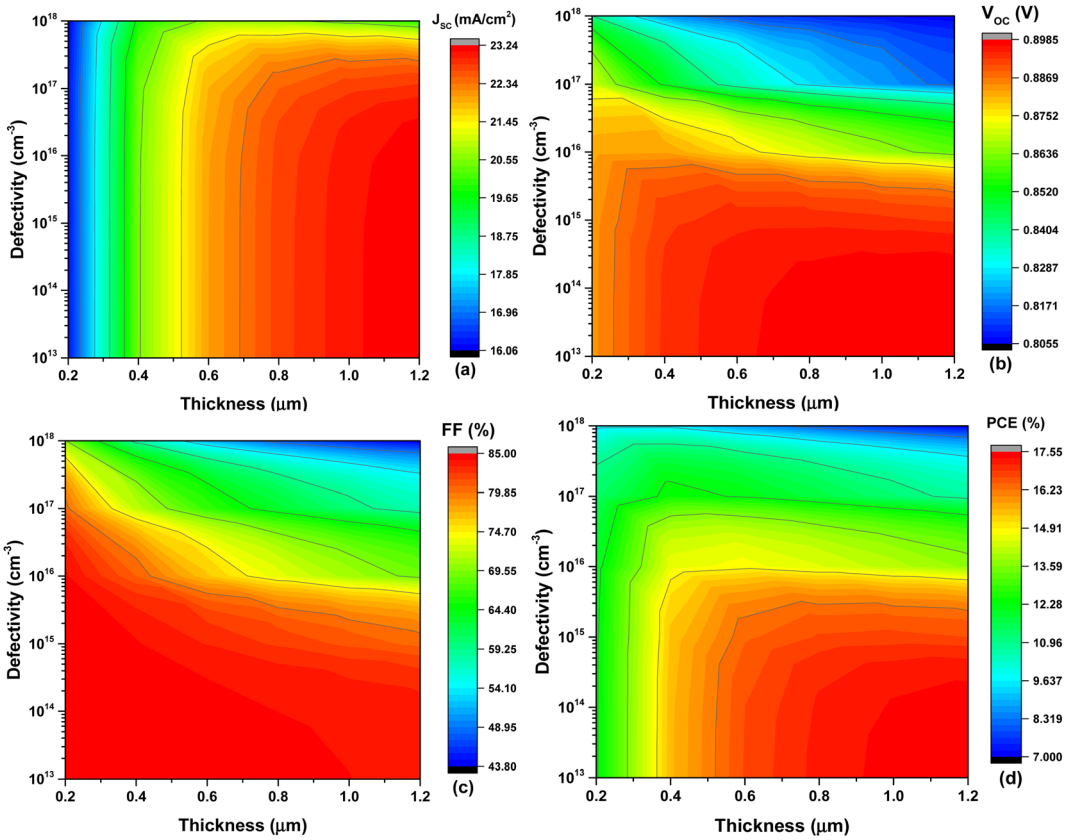

Fig. 4 The contour plotting of the perovskite material *i.e.,* $MAPbI_3$ for high output parameters at the optimized temperature and doping conditions.

μm, and the compatible thicknesses for the optimal efficiency of the simulated device were determined. As shown in Fig. 2a, for $MAPbI_3$, the short-circuit current density (J_{SC}) rises from 16 mA cm^{-2} and reaches the maximum point at 22 mA cm^{-2} as the PAL thickness increases from 0.2 μm to 1.2 μm. This is due to the absorption rate's proportional dependence on current density. J_{SC} remains constant, *i.e.*, ~21 mA cm^{-2} and 8 mA cm^{-2} for $MAPbI_2Br$ and $MAPbBr_3$ throughout the active layer thickness of 1.2 μm, respectively. Fig. 2b depicts the variation in V_{OC} of all three Perovskite materials and the active layer thickness, which ranges from 0.2 μm to 1.2 μm. The device's V_{OC} is at a steady state with increasing thickness inside the PSC. In terms of numbers, the 1.2 μm thick $MAPbBr_3$-PA has a higher V_{OC} value of 1.52 Volt. The devices in Fig. 2c demonstrate the Fill Factor (FF) property. The Fill factor indicates the squareness of the *J–V* curve and indicates the resistive losses in the device, and higher FF ensures higher output power and conversion efficiency as both the parameters are proportional to each other. The FF of $MAPbI_3$ decreases from 87.2% to 86.9%, while the PAL thickness increases from 0.2 μm to 1.2 μm. Among the three Perovskite materials used, the material $MAPbI_2Br$ shows the maximum value. For $MAPbI_2Br$, the FF appears to remain constant, at around 86.2%, and the FF of $MAPbBr_3$ decreases from 87.89% to 86.89% for the PAL thicknesses varying from 0.2 μm to 1.2 μm, respectively. While Fig. 2d depicts PCE, the most crucial feature of the PSC. The PCE of $MAPbI_3$ remains at approximately 17.62% under the said variation of PAL and the PCE of $MAPbBr_3$ eventually reached 9.85% after steadily rising from 5.2% for the thickness values varying from 0.2 μm to 1.2 μm. The PCE of the material $MAPbI_2Br$ rises from 14.8% to 22.05% at the maximum thickness level of the perovskite material. It can be noted from the data in Fig. 2d that the increase in PCE is significant during the initial rise in the thickness of the PAL. This is due to an improvement in photon absorption at higher thicknesses which results in an improvement in J_{SC} and PCE. The same can be validated through J_{SC}. However, further increasing the thickness from 1.0 to 1.2 μm the improvement is not that prominent, and the FF trend showed degradation at higher thicknesses. So eventually a saturated J_{SC} and reduced FF will reduce the PCE if PAL thickness is increased beyond a certain limit. The current work offers a better outcome than the previous work by Dipta *et al.*[64]

3.2 The influence of the temperature on the PSC outputs

Fig. 3a and b depicts a comprehensive examination of the PSC properties as temperature changes. As depicted in Fig. 3(a–d), the four parameters J_{SC}, V_{OC}, FF, and PCE decrease as the temperature rises from 300 K–400 K for the Perovskite material $MAPbI_2Br$. The maximum values for the Perovskite $MAPbI_2Br$ parameters are 21.91 mA cm^{-2}, 1.16 V, 86.89%, and 22.05% at 300 K.

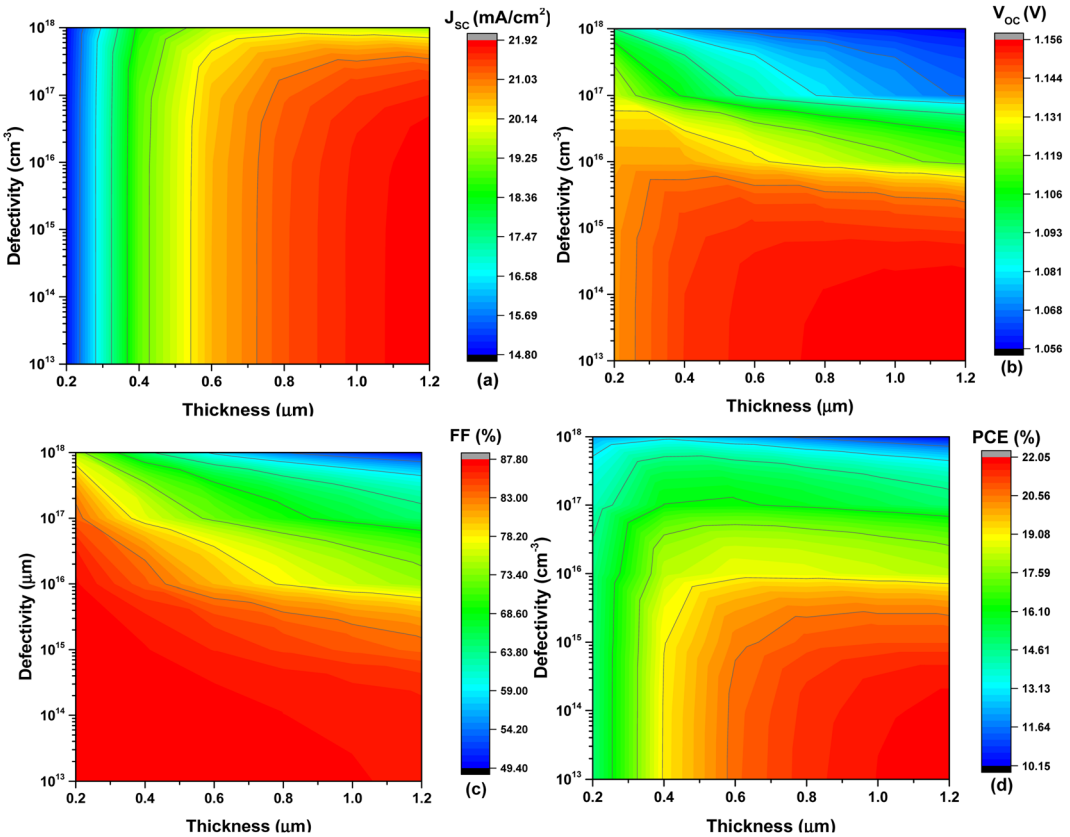

Fig. 5 The contour plotting of the perovskite material, *i.e.*, $MAPbI_2Br$, for high output parameters at the optimized temperature and doping conditions.

For the $MAPbBr_3$, the values of parameters V_{OC} and FF both decrease as the temperature rises from 300 K–400 K, with the maximum values at 300 K being 0.90 V and 81%, respectively. While the value of the parameter J_{SC} rises from 16.6 mA cm^{-2} to 17.4 mA cm^{-2} as the temperature increases from 300 K to 400 K, in contrast, PCE remains nearly constant at approximately 9.8% as the temperature increases to the maximum value. Since the increase in temperature reduces the V_{OC} of the PSC devices. As we know, due to the decrease in V_{OC}, the *J*–*V* curve becomes steeper, as a result, the FF value is increased as compared to other PSC devices. This is the reason for a nonlinear increase in FF for $MAPbBr_3$-based PSC. And for the material $MAPbI_3$, values of the three parameters J_{SC}, FF, and PCE decrease with increasing temperature from 300 K to 400 K with values of 20.7 mA cm^{-2}, 62%, and 20.8% at peak for the respective parameters at 300 K, but the value of the parameter V_{OC} for the $MAPbI_3$ appears to remain unchanged with a value of 0.982 V while the temperature increases. The current simulation offers an improvement in overall output parameters as compared to the previous work by Bhattarai *et al.*[65]

3.3 The combined influence of thickness and total defect density using contour plotting

There are three perovskites devices: firstly, the $MAPbI_3$-based PSC. As Fig. 4 shows the contour plot over the perovskite material's thicknesses and total defect density. The following outcomes can be deduced. Firstly, the PCE is maximum at 1.2 μm thickness and defectivity of 1×10^{13} cm^{-3}, which offers a high value of PCE, *i.e.*, nearly 17.5%. The V_{OC}, on the other hand, is at its maximum, with a value of 1.144 V at 0.2 μm thickness and 1×10^{13} cm^{-3} defectivity. While the J_{SC} keeps on increasing with the increase in thickness and reduces when the defectivity is higher. The maximum J_{SC} value is 21.03 mA cm^{-2} at a thickness of 1.2 μm and with a defectivity of 1×10^{18} cm^{-3}. Lastly, the maximum FF is found to be 83% at thickness 0.2 μm thickness and defectivity 1×10^{18} cm^{-3}, respectively.

The second PSC device with the perovskite material of $MAPbI_2Br$ offers outstanding device outputs as depicted in Fig. 5. Firstly, the PCE is maximum at 1.2 μm thickness and 1×10^{13} cm^{-3}, which offers a high value of PCE, *i.e.*, nearly a value of 22.05%. On the other hand, the V_{OC} is at maximum with the value of 1.156 V at the higher thickness regions and low defect density region, *i.e.*, 1×10^{13} cm^{-3} defectivity. At the same time, the J_{SC} keeps on increasing with higher thickness levels and smaller defectivity of the PAL. The maximum J_{SC} value is 21.93 mA cm^{-2} at a thickness of 1.2 μm and with a defectivity of 1×10^{13} cm^{-3}. Lastly, the maximum FF is found to be 87.80% at a thickness of 1.2 μm and defectivity of 1×10^{18} cm^{-3}, respectively. It can be observed that the four parameters are more predominant for the $MAPbI_2Br$-based PSC as compared to other perovskite materials.

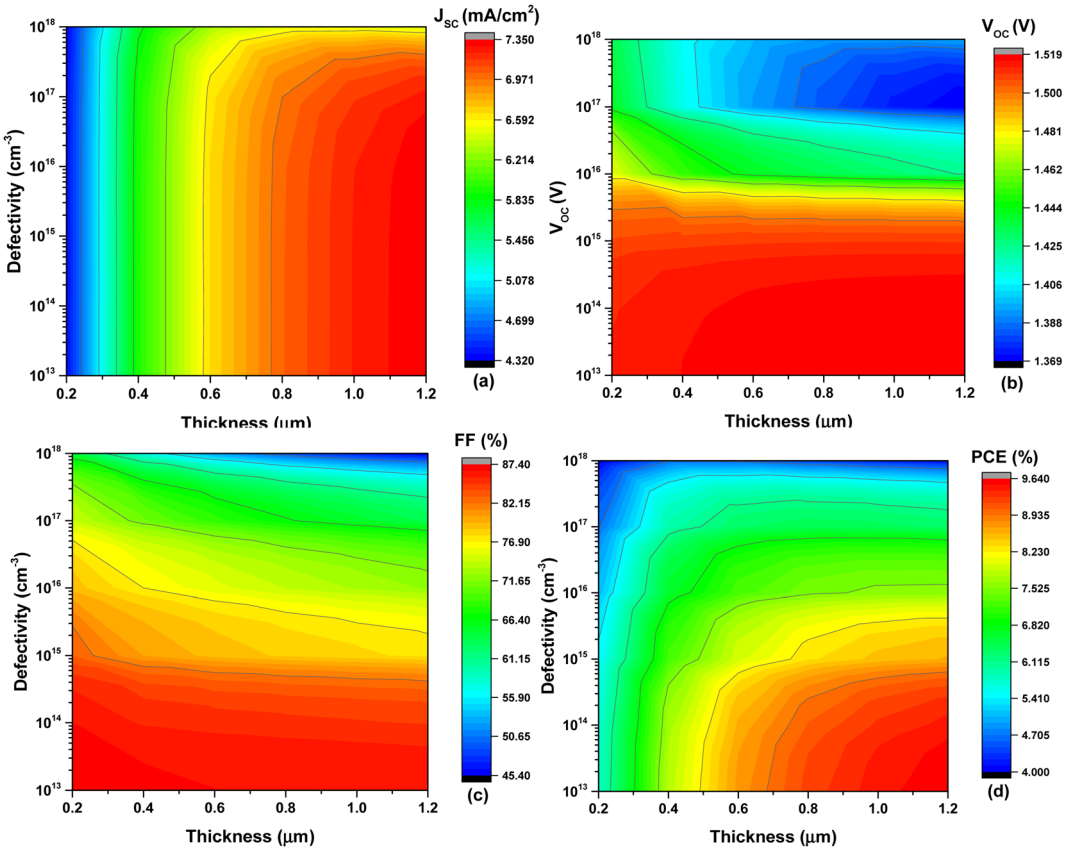

Fig. 6 The contour plotting of the perovskite material *i.e.*, $MAPbBr_3$, for high output parameters at the optimized temperature and doping conditions.

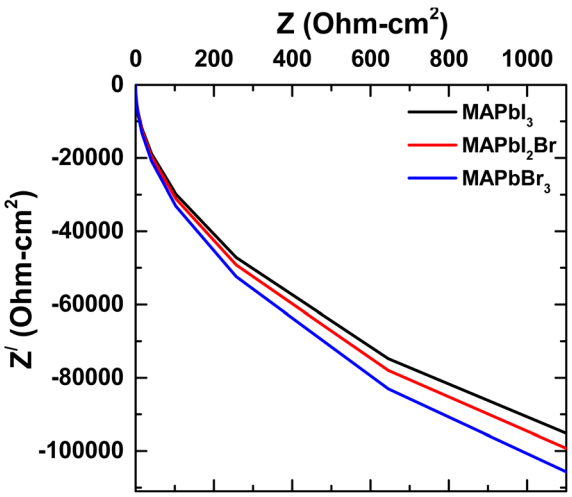

Fig. 7 The comparison of impedance (real *vs.* imaginary) for all three perovskites.

Fig. 6 depicts how the PCE value continues to increase with the thickness and defectivity for $MAPbBr_3$-based PSC. The maximum value of PCE is 8.935% found at 1.2 μm thickness and 1×10^{13} cm^{-3} defectivity. While the maximum value of V_{OC} is 1.500 V found at a thickness of 0.2 micrometer and defectivity of 1×10^{13} cm^{-3}, whereas J_{SC} increases with increasing thickness and defectivity, reaching a maximum of 6.971 mA cm^{-2} at 1.2 μm thickness, and 1×10^{18} cm^{-3} defectivity. Lastly, the peak value of FF is 82.15%, which is found at 1.2 μm thickness and defectivity 1×10^{18} cm^{-3}. Similar outcomes can be obtained from the previous SCAPS simulated work of Bhattarai *et al.*[66]

3.4 Comparison of impedances of the PSCs

The impedance analysis is one of the better ways to understand the behavior of the perovskite materials having distinct halides. From Fig. 7, it is evident that the highest value of impedance is reached for the $MAPbBr_3$ perovskite, *i.e.*, almost more than 100 000 ohm cm^2. While the Cl_2Br-based offers almost nearly 100 000 ohm cm^2, I-based Perovskite offers 95 000 ohm cm^2. The previous study also offers a similar impedance value, as depicted in Fig. 8. The report by Bhattarai *et al.* provides a high value nearly identical to the value obtained in this analysis.[67] The impedance plot or Nyquist plot of a solar cell provides a detailed qualitative understanding of resistive losses, capacitance, and recombination rate defects in the device. The impedance curve reported in Fig. 7 shows a similar trend in all three devices with minor changes.

3.5 Comparison of QE and *J–V* of the PSCs

The following points are attained from the *J–V* curve shown in Fig. 8. The $MAPbBr_3$ perovskite attains the highest V_{OC}, nearly

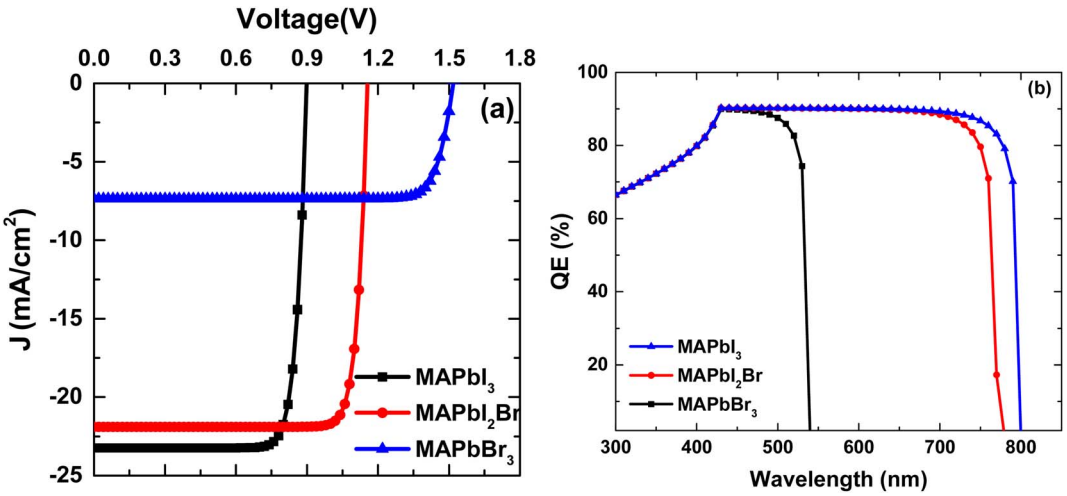

Fig. 8 The comparison of *J*–*V* and QE of the different perovskite materials.

Table 3 The overall assessment of the present work with the prior works

Device structures	J_{SC} (mA cm^{-2})	V_{OC} (V)	FF (%)	PCE (%)
$MAPbI_3$-based PSC	23.24	0.898	83.95	17.53
$MAPbBr_3$-based PSC	7.34	1.52	86.23	9.62
$MAPbI_2Br$-based PSC	21.91	1.16	86.89	22.05
Jayan *et al.*[48]	21.83	1.00	71.19	15.55
Dipta *et al.*[64]	16.27	1.06	76.22	13.03

1.5 V, and J_{SC} of 12.5 mA cm^{-2}. Though the V_{OC} is high, the J_{SC} is very low to contribute PCE as the V_{OC} and J_{SC} are directly proportional to the efficiency. On the contrary, the $MAPbI_3$-based PSC offers the smallest value of V_{OC}, which is unsuitable for better efficiency. The $MAPbI_3$ attains the highest V_{OC} of 0.9 V and 23 mA cm^{-2} value of J_{SC} as shown in Fig. 8a. Since the need of obtaining the best combination of V_{OC} and J_{SC} is mainly necessary. The $MAPbI_2Br$ attains the highest V_{OC} of 1.1 V and 22 mA cm^{-2} of J_{SC}, which offers an excellent efficiency value. The result can be compared with previous work by Adhikari *et al.*[68] The *J*–*V* curve of $MAPbI_2Br$ also shows that a higher value of FF can be reached, as the steep curve of *J*–*V* is higher than the other two materials for better efficiency.

As from the QE curve in Fig. 8b, it is found that all three perovskites show high QE values. Comparatively, the highest bandgap perovskite of $MAPbBr_3$ drops at a very small wavelength of nearly 540 nm as the dependency of QE is reciprocal to each other. The lowest bandgap material of $MAPbI_3$ drops at the highest point of wavelength, *i.e.*, nearly 800 nm, as the bandgap is almost 1.5 eV ($MAPbI_3$). The result can be matched with the previous work by Jayan *et al.*[48] The overall comparison of the present work with the previous works is reported in Table 3.

4. Conclusions

The simulation and investigation of the PSC structure with different perovskite materials having a configuration of ITO/WO_3/PAL/Mg-CuCrO2/Ag have been utilized using SCAPS-1D simulating software. The WO_3 has been used as ETL, keeping in view of maximizing the suitable band alignment and higher mobility of the carrier with the perovskite material in the solar devices, whereas, for the collection of the holes, Mg–$CuCrO_2$ as the HTL for the numerical simulation of the PSC device. Distinctive halide-based methylammonium-based perovskites are used as active PAL that shows a greater influence on the output parameter than the e–h transport layers of the PSC device. So, the optimization of the absorber's thicknesses for the PSC is carried out for better outputs. The work attained an optimal absorber thickness of 1.2 μm for the $MAPbI_2Br$-based PSC device. The defectivity of the PSC shows that at the level of 1×10^{13} cm^{-3}, which obtains higher outputs. Moreover, the study also includes the impact of the resistances for enhancing the higher efficiency of the PSC device. The simulation clearly exhibits that the $MAPbI_2Br$ can provide excellent outputs, as in the present case, nearly 22.05%, which may be a fascinating and suitable option in developing the PSC device. The overall conclusion of the present study thus may offer valuable contribution regarding the manufacturing of more efficient $MAPbI_2Br$-based PSC devices. It is also worth to note that the SCAPS-1D simulator used in this work is applicable to one-dimensional devices and cannot support complex device geometry. Therefore, advanced device simulators can also be considered in future work.

Data availability

The raw/processed data required to reproduce these findings cannot be shared at this time as the data also forms part of an ongoing study.

Conflicts of interest

The authors declare that they have no known competing financial interests or personal relationships that could have appeared to influence the work reported in this paper.

Acknowledgements

The authors have extended their appreciation to the Deanship of Scientific Research at King Khalid University, Saudi Arabia for funding this work through Research Groups Program under grant number R.G.P.2: 219/44. The SCAPS-1D program was kindly provided by Dr M. Burgelman of the University of Gent in Belgium. The authors would like to express their gratitude to him.

References

1 S. Bhattarai, A. Mhamdi, I. Hossain, Y. Raoui, R. Pandey, J. Madan, A. Bouazizi, M. Maiti, D. Gogoi and A. Sharma, *Micro Nanostruct.*, 2022, **172**, 207450.
2 S. Karthick, S. Velumani and J. Bouclé, *Opt. Mater.*, 2022, **126**, 112250.
3 F. Azri, A. Meftah, N. Sengouga and A. Meftah, *Sol. Energy*, 2019, **181**, 372–378.
4 R. Pandey, J. Madan and R. Sharma, *IEEE Trans. Electron Devices*, 2021, **68**, 1757–1763.
5 R. Pandey, S. Bhattarai, K. Sharma, J. Madan, A. K. Al-Mousoi, M. K. A. Mohammed and M. K. Hossain, *ACS Appl. Electron. Mater.*, 2023, **5**(6), 2431–2460.
6 D. Muchahary, S. Bhattarai, A. K. Mahato and S. Maity, in *Emerging Materials*, Springer Nature Singapore, Singapore, 2022, pp. 361–406.
7 C. Devi and R. Mehra, *J. Mater. Sci.*, 2019, **54**, 5615–5624.
8 N. Gamal, S. H. Sedky, A. Shaker and M. Fedawy, *Optik*, 2021, **242**, 167306.
9 D. Muchahary, L. S. Ram, R. Narzary, P. P. Sahu, S. Bhattarai and S. Tayal, *Curr. Appl. Phys.*, 2022, **38**, 15–21.
10 F. H. Isikgor, S. Zhumagali, L. V. T. Merino, M. De Bastiani, I. McCulloch and S. De Wolf, *Nat. Rev. Mater.*, 2023, **8**, 89–108.
11 A. S. R. Bati, Y. L. Zhong, P. L. Burn, M. K. Nazeeruddin, P. E. Shaw and M. Batmunkh, *Commun. Mater.*, 2023, **4**, 2.
12 Z. Zhang, L. Qiao, K. Meng, R. Long, G. Chen and P. Gao, *Chem. Soc. Rev.*, 2023, **52**, 163–195.
13 S. Bhattarai and T. D. Das, *Opt. Mater.*, 2021, **111**, 110661.
14 S. Bhattarai and T. D. Das, *Sol. Energy*, 2021, **217**, 200–207.
15 H. Bencherif, F. Meddour, M. H. Elshorbagy, M. K. Hossain, A. Cuadrado, M. A. Abdi, T. Bendib, S. Kouda and J. Alda, *Micro Nanostruct.*, 2022, **171**, 207403.
16 W. S. Yang, B.-W. W. Park, E. H. Jung, N. J. Jeon, Y. C. Kim, D. U. Lee, S. S. Shin, J. Seo, E. K. Kim, J. H. Noh and S. Il Seok, *Science*, 2017, **356**, 1376–1379.
17 K. Fatema and M. S. Arefin, *Opt. Mater.*, 2022, **125**, 112036.
18 P. Srivastava, Sadanand, S. Rai, P. Lohia, D. K. Dwivedi, H. Qasem, A. Umar, S. Akbar, H. Algadi and S. Baskoutas, *Phys. Scr.*, 2022, **97**, 125004.
19 A. Kojima, K. Teshima, Y. Shirai and T. Miyasaka, *J. Am. Chem. Soc.*, 2009, **131**, 6050–6051.
20 G. Pindolia, S. M. Shinde and P. K. Jha, *Mater. Chem. Phys.*, 2023, **297**, 127426.
21 A. Thakur, D. Singh and S. Kaur Gill, *Mater. Today: Proc.*, 2022, **71**, 195–201.
22 S. Mushtaq, S. Tahir, A. Ashfaq, R. Sebastian Bonilla, M. Haneef, R. Saeed, W. Ahmad and N. Amin, *Sol. Energy*, 2023, **249**, 401–413.
23 S. Bhattarai, A. Sharma, P. K. Swain and T. D. Das, *J. Electron. Mater.*, 2021, **50**, 6756–6765.
24 S. Bhattarai, A. Sharma, D. Muchahary, M. Gogoi and T. D. Das, *Optik*, 2021, **243**, 167492.
25 M. K. Hossain, M. K. A. Mohammed, R. Pandey, A. A. Arnab, M. H. K. Rubel, K. M. Hossain, M. H. Ali, M. F. Rahman, H. Bencherif, J. Madan, M. R. Islam, D. P. Samajdar and S. Bhattarai, *Energy Fuels*, 2023, **37**, 6078–6098.
26 T. Dureja, A. Garg, S. Bhalla, D. Bhutani and A. Khanna, *Mater. Today: Proc.*, 2022, **71**, 239–242.
27 Y. Raoui, H. Ez-Zahraouy, N. Tahiri, O. El Bounagui, S. Ahmad and S. Kazim, *Sol. Energy*, 2019, **193**, 948–955.
28 A. K. Al-Mousoi, M. K. A. Mohammed, A. Kumar, R. Pandey, J. Madan, D. Dastan, M. K. Hossain, P. Sakthivel, G. Anandha babu and Z. M. Yaseen, *Phys. Chem. Chem. Phys.*, 2023, **25**, 16459–16468.
29 N. Shrivastav, J. Madan, M. K. A. Mohammed, M. K. Hossain and R. Pandey, *Mater. Res. Express*, 2023, **10**, 075506.
30 D. Dastan, M. K. A. Mohammed, A. K. Al-Mousoi, A. Kumar, S. Q. Salih, P. S. JosephNg, D. S. Ahmed, R. Pandey, Z. M. Yaseen and M. K. Hossain, *Sci. Rep.*, 2023, **13**, 9076.
31 R. Pandey, A. Khanna, K. Singh, S. K. Patel, H. Singh and J. Madan, *Sol. Energy*, 2020, **207**, 893–902.
32 H. Xiao, C. Zuo, K. Yan, Z. Jin, Y. Cheng, H. Tian, Z. Xiao, F. Liu, Y. Ding and L. Ding, *Adv. Energy Mater.*, 2023, **13**, 2300738.
33 S. Bhattarai, M. K. Hossain, R. Pandey, J. Madan, D. P. Samajdar, M. F. Rahman, M. Z. Ansari and M. Amami, *Energy Fuels*, 2023, **37**(14), 10631–10641.
34 N. Shrivastav, J. Madan, M. K. A. Mohammed, M. K. K. Hossain, R. Pandey, M. K. A. Mohammed, M. K. K. Hossain and R. Pandey, *Mater. Res. Express*, 2023, **10**, 075506.
35 R. L. Milot, G. E. Eperon, T. Green, H. J. Snaith, M. B. Johnston and L. M. Herz, *J. Phys. Chem. Lett.*, 2016, **7**, 4178–4184.
36 S. J. Lee, S. S. Shin, Y. C. Kim, D. Kim, T. K. Ahn, J. H. Noh, J. Seo and S. Il Seok, *J. Am. Chem. Soc.*, 2016, **138**, 3974–3977.
37 H. Ban, T. Nakajima, Z. Liu, H. Yu, Q. Sun, L. Dai, Y. Shen, X.-L. Zhang, J. Zhu, P. Chen and M. Wang, *J. Mater. Chem. A*, 2022, **10**, 3642–3649.
38 S. Abdelaziz, A. Zekry, A. Shaker and M. Abouelatta, *Opt. Mater.*, 2020, **101**, 109738.
39 C. Li, X. Wang, E. Bi, F. Jiang, S. M. Park, Y. Li, L. Chen, Z. Wang, L. Zeng, H. Chen, Y. Liu, C. R. Grice, A. Abudulimu, J. Chung, Y. Xian, T. Zhu, H. Lai, B. Chen, R. J. Ellingson, F. Fu, D. S. Ginger, Z. Song, E. H. Sargent and Y. Yan, *Science*, 2023, **379**, 690–694.
40 M. K. Hossain, G. F. I. I. Toki, I. Alam, R. Pandey, D. P. Samajdar, M. F. Rahman, M. R. Islam, M. H. K. K. Rubel, H. Bencherif, J. Madan and M. K. A. A. Mohammed, *New J. Chem.*, 2023, **47**, 4801–4817.

41 N. Shrivastav, S. Kashyap, J. Madan, A. K. Al-Mousoi, M. K. A. Mohammed, M. K. Hossain, R. Pandey and J. Ramanujam, *Energy Fuels*, 2023, **37**, 3083–3090.
42 S. Bhattarai, R. Pandey, J. Madan, A. Mhamdi, A. Bouazizi, D. Muchahary, D. Gogoi, A. Sharma and T. D. Das, *IEEE Trans. Electron Devices*, 2022, **69**, 3217–3224.
43 D. Cao, Z. Li, W. Li, K. Pei, X. Zhang, L. Wan, L. Zhao, A. Cherevan, D. Eder and S. Wang, *Mater. Chem. Front.*, 2023, **7**, 964–974.
44 S. Brittman and E. C. Garnett, *J. Phys. Chem. C*, 2016, **120**, 616–620.
45 S. Mehra, R. Pandey, J. Madan, R. Sharma, L. Goswami, G. Gupta, A. K. Srivastava and S. Sharma, *SSRN Electron. J.*, 2022, DOI: **10.2139/ssrn.4189425**.
46 R. Singh, M. Parashar, S. Sandhu, K. Yoo and J.-J. Lee, *Sol. Energy*, 2021, **220**, 43–50.
47 D. K. Sarkar, M. Mottakin, A. K. M. Hasan, V. Selvanathan, S. Khan, M. N. I. Khan, A. F. M. Rabbani, M. Shahinuzzaman, M. Aminuzzaman, F. H. Anuar, T. Suemasu, K. Sopian and M. Akhtaruzzaman, *SSRN Electron. J.*, 2023, DOI: **10.2139/ssrn.4236191**.
48 K. D. Jayan and V. Sebastian, *Semicond. Sci. Technol.*, 2021, **36**, 065010.
49 M. Kumar, A. Raj, A. Kumar and A. Anshul, *Opt. Mater.*, 2020, **108**, 110213.
50 G. Pindolia, S. M. Shinde and P. K. Jha, *Sol. Energy*, 2022, **236**, 802–821.
51 M. K. Hossain, G. F. Ishraque Toki, D. P. Samajdar, M. H. K. Rubel, M. Mushtaq, M. R. Islam, M. F. Rahman, S. Bhattarai, H. Bencherif, M. K. A. Mohammed, R. Pandey and J. Madan, *Energy Fuels*, 2023, **37**, 7380–7400.
52 K. Chakraborty, M. G. Choudhury and S. Paul, *Sol. Energy*, 2019, **194**, 886–892.
53 S. Bhattarai, R. Pandey, J. Madan, Z. Ansari, M. K. Hossain, M. Amami, S. H. Ahammad and A. N. Z. Rashed, *Prog. Photovoltaics Res. Appl. Res. Appl.*, 2023, DOI: **10.1002/pip.3732**.
54 N. Shrivastav, J. Madan, M. K. A. Mohammed, A. K. Al-Mousoi, M. K. Hossain, M. Amami, M. F. Rahman, D. P. Samajdar, S. Bhattarai and R. Pandey, *Mater. Today Commun.*, 2023, **36**, 106761.
55 S. Bhattarai, D. Jayan, A. Yousfi, M. Chowdhury, M. F. Rahman, R. Pandey, J. Madan, Z. Ansari and M. K. Hossain, *Phys. Scr.*, 2023, **98**(9), 095507.
56 M. K. Hossain, G. F. I. Toki, D. P. Samajdar, M. Mushtaq, M. H. K. Rubel, R. Pandey, J. Madan, M. K. A. Mohammed, M. R. Islam, M. F. Rahman and H. Bencherif, *ACS Omega*, 2023, **8**, 22466–22485.
57 S. Ahmed, F. Jannat, M. A. K. Khan and M. A. Alim, *Optik*, 2021, **225**, 165765.
58 S. Kashyap, J. Madan, M. K. A. Mohammed, M. K. Hossain, S. Ponnusamy and R. Pandey, *Mater. Lett.*, 2023, **339**, 134096.
59 S. Abdelaziz, A. Zekry, A. Shaker and M. Abouelatta, *Opt. Mater.*, 2020, **101**, 109738.
60 S. Karthick, S. Velumani and J. Bouclé, *Sol. Energy*, 2020, **205**, 349–357.
61 K. Tan, P. Lin, G. Wang, Y. Liu, Z. Xu and Y. Lin, *Solid-State Electron.*, 2016, **126**, 75–80.
62 M. K. Hossain, M. S. Uddin, G. F. I. Toki, M. K. A. Mohammed, R. Pandey, J. Madan, M. F. Rahman, M. R. Islam, S. Bhattarai, H. Bencherif, D. P. Samajdar, M. Amami and D. K. Dwivedi, *RSC Adv.*, 2023, **13**, 23514–23537.
63 M. K. A. Mohammed, A. K. Al-Mousoi, A. Kumar, M. M. Sabugaa, R. Seemaladinne, R. Pandey, J. Madan, M. K. Hossain, B. S. Goud and A. A. Al-Kahtani, *J. Alloys Compd.*, 2023, **963**, 171246.
64 S. S. Dipta, A. Uddin and G. Conibeer, *Heliyon*, 2022, **8**, e11380.
65 S. Bhattarai, R. Pandey, J. Madan, D. Muchahary and D. Gogoi, *Sol. Energy*, 2022, **244**, 255–263.
66 S. Bhattarai, R. Pandey, J. Madan, F. Ahmed and S. Shabnam, *Mater. Today Commun.*, 2022, **33**, 104364.
67 S. Bhattarai, A. Sharma and T. D. Das, *Optik*, 2020, **224**, 165430.
68 K. R. Adhikari, S. Gurung, B. K. Bhattarai and B. M. Soucase, *Phys. Status Solidi C*, 2016, **13**, 13–17.